Molecular Aggregation of Aluminum Phthalocyanine Chloride in Organic and Water-Organic Media

Inna V. Klimenko[1*], Tatiana Yu. Astakhova[1], Elena N. Timokhina[1], and Anton V. Lobanov[1,2]

[1] N.M. Emanuel Institute for Biochemical Physics Russian Academy of Sciences, 4 Kosygin str., Moscow 119334, Russia

[2] N.N. Semenov Federal Research Center for Chemical Physics, Russian Academy of Sciences, 4 Kosygin str., Moscow 119991, Russia

***e-mail:** inna@deom.chph.ras.ru

Abstract. The process of aluminum phthalocyanine chloride (AlClPc) aggregation in water and water-organic media was studied both by quantum mechanical theoretical calculations and experimental methods of optical absorption and fluorescence spectroscopy. The structures of AlClPc in the monomeric and dimerized (H- and J-aggregates) states in the gas phase and in both N,N-dimethylformamide (DMF) and DMF-water binary solution were calculated by the electron density functional theory (DFT) method. The absorption and fluorescence spectra of these structures were calculated in time-dependent electron DFT approximation. Comparing all data obtained, conclusions about the change in the aggregation state of AlClPc were drawn. Results demonstrate depending AlClPc photophysical parameters on its monomer/dimer ratio in solution, which is determined by concentration of the dye and water in the system. The experimental results obtained for water-organic medium indicate the existence of a critical water concentration (~ 7.8 %), at which the ratio of monomers and dimers (J-aggregates) of AlClPc changes dramatically. In AlClPc-DMF system the dye is completely in monomeric form. The results of the study make it possible to predict the aggregation behavior of AlClPc complexes in water-organic media, as well as to control and manage their aggregation behavior.

Keywords: aluminum phthalocyanine chloride; water-organic media; aggregation process; theoretical calculations; dimers; photophysical properties.

Paper #8120 received 27 Feb 2023; revised manuscript received 1 Jun 2023; accepted for publication 2 Jun 2023; published online 9 Jul 2023. doi: 10.18287/JBPE23.09.030301.

1 Introduction

Photodynamic therapy (PDT) is one of the most promising methods among the clinical treatments for cancer including surgery, radiation therapy, chemotherapy, and immunotherapy. PDT involves a combination of visible light and a photosensitizer (Ps), natural or artificially synthesized photoactive compound. Ps can selectively accumulate in target tissues and generate singlet oxygen or oxygen-containing free radicals when locally irradiated with the light of a certain wavelength, usually a red laser beam, corresponding to the maximum absorption of Ps. Singlet oxygen $^1O_2$ and other active forms of oxygen $O_2^{-\bullet}$, $OH^\bullet$, and H_2O_2, (cytotoxic reactive oxygen species, ROS) play a key role in photodynamic process. They are responsible for oxidative biological damage that destroys vital organelles of tumour cells and leads to cell death and, as a result, to necrosis, apoptosis, or autophagy of the target tissue [1–9].

Currently, significant efforts are focused on advancing PDT by improving drug delivery systems and developing new perfect photosensitizers. In this regard, phthalocyanines (Pc) discovered by Braun and Tcherniac [10] represent a dynamic research field and offer great opportunities due to their magnificent

photophysical and photochemical properties, structural versatility, and stability. All Pc are intensely coloured two-dimensional tetrapyrrolic macroheterocyclic compounds with particular electronic delocalization of the 18-π aromatic system. They display good absorption in the UV-Vis region, namely, the B-band region at 300–400 nm and the Q-band region at 600–700 nm (the so-called "therapeutic window" that guarantees maximum tissue penetration). They also have a long lifetime in the triplet state (0.1–1 ms) and a high quantum yield of singlet oxygen (Φ_Δ = 9.1) [11–19].

The synthetic Pc molecule, related to tetraazaporphyrins (porphyrazines), consists of four pyrrole subunits, which are linked by four nitrogen atoms, similar to the macrocycle of porphyrazines. It is disposed to be integrated with a metal atom (d^0- and d^{10}-configurations) in the central cavity to form metal phthalocyanine complexes (MePc) [20–24]. This central coordinated metal atom can be one of at least 70 different elements of the periodic table [25], and MePc were developed similarly to the biologically important class of porphyrins and can be synthesized through metal-template directed cyclotetramerization between a phthalocyanine precursor (phthalonitriles) and the corresponding metal salt [25].

When complexed with metal, the geometries as well as the electronic and other desirable properties of Pc can be improved. When the central metal atom is diamagnetic or a nontransition metal element, MePc are considered to be more efficient sensitizers owing to their high triplet state quantum yields and long triplet lifetimes [26, 27]. MePc are very interesting substances for biomedical analysis because of easy detection of their changed photophysical properties when treated with biologically significant compounds such as volatile organic compounds, for example, alcohol and aldehyde vapors [28]. Also, the type of central metal ions is a key factor affecting the catalytic activity of MePc [29–31].

The optical properties of MePc also depend on the type of a solvent. For example, the maximum absorption wavelength of MePc weakly correlates with the polarity of the solvent, but it is sensitive to the very structure of the solvent molecules [32]. It is known [33] that N,N-dimethylformamide (DMF), a polar aprotic solvent, interacts with the central metal cation of Pc macrocycle through the double-bonded oxygen atom that can explain high DMF solvation. Also, the highest solvation ability of DMF to Pc can be caused by its donor-acceptor properties [33]. The addition of water to the DMF solution changes the absorption spectrum of Pc. The aggregation of the metal complex also increases with the increase in the percentage of water in the system [34].

Moreover, DMF is a hepatotoxic agent with unique antibacterial and antiviral properties. It is frequently used in safe concentrations as a solvent for pharmceutical, biomedical, and chemical applications because of its unique solvency parameters, for example, when synthesizing sulfadiazine, cortisone, and vitamin B_6 [35, 36]. DMF-water solution is often used as a liquid medium for obtaining platform for drug delivery process [37–39] and can be used as a solvent (in small doses) when receiving drugs for antibacterial and photodynamic therapy.

It is very critical to have MePc molecules in monomeric (isolated) form for their effective functioning as photosensitizers for PDT. In this case, there is no self-quenching of triplet excited states, which leads to efficient triplet energy transfer to the oxygen molecule and triggering the mechanism of photodynamic action [40]. However, for medical diagnostics, it is extremely important to use MePc without any adverse phototoxic properties [40, 41].

Phthalocyanines, like other tetrapyrrolic compounds, have a strong tendency to stacking (self-aggregation) with the formation of dimers and other types of aggregates in water or water solutions, which reduce photodynamic activity of MePc. The degree of aggregation depends on various parameters such as Pc concentration, a central coordinated metal, a solvent type, and substituents in the side chain. The self-aggregation of Pc occurs due to π-π interactions between the aromatic systems of Pc; specific interactions between the metal ligand and solvent molecules are also possible [17, 42, 43]. Aggregation of MePc in water solutions can occur due to hydrogen bonds between the atoms of MePc and water molecules [16, 17, 42, 44].

Various methods are used to prevent the aggregation of MePc complexes in water/biological systems and bodily fluids [8, 24, 45–52]. The modification of the Pc macro ring by replacing peripheral and/or nonperipheral hydrogen atoms with various substituents (alkyl, aryl, alkoxy, and aryloxy), the synthesis of one-dimensional crystals of MePc nanowires to increase the dispersibility of Pc in water, the synthesis of phthalogen conjugates with carbohydrates and the formation of related MePc complexes with carbohydrates, immobilization of Pc on the surface of an inert solid support are among them. Various drug delivery systems are also used to transport Pc to targets, such as liposomal and micellar media, magnetic emulsion with nanostructured colloidal particles and biocompatible polymer nanoparticles, etc.

In order to reduce hydrophobicity and Pc aggregation in water and water solutions, the authors recently proposed to use a theranostic two-dimensional (2D) nano carbon material, oxygen-free graphene, as a part of hybrid systems in conjunction with phthalocyanine. The synthesis of hybrid structures based on oxygen-free graphene and MePc complex – aluminum phthalocyanine chloride (AlClPc, $C_{32}H_{16}AlClN_8$) was reported [17, 53]. It was found that the coordinating interaction of graphene with AlClPc prevents the aggregation of the latter and stabilizes it as a chemically active monomer. Moreover, AlClPc in combination with oxygen-free graphene exhibited a high PD effect.

Thus, the search for new MePc complexes with low aggregation in water and physiological solutions is of current interest. An effective search requires an understanding of the mechanisms of interchromoform interaction in water and water solutions. In this paper in the development of the topic and in order to evaluate the

possibility of changing the physicochemical properties of AlClPc, we carried out the theoretical and experimental studies of the AlClPc complex aggregation in DMF and DMF-water solution with different concentration of water. Aggregation was controlled experimentally by the optical absorption and fluorescence spectra. Quantum chemical methods were used to evaluate all possible AlClPc structures. The adsorption and fluorescence spectra of these structures were calculated in time-dependent electron Density Functional Theory (DFT) approximation. By comparing the experimental and theoretically calculated spectra, conclusions were drawn about the change in the aggregation state of AlClPc depending on the water concentration.

2 Materials and Methods

2.1 Theoretical Calculations; Methods

Quantum chemical calculations were performed with ORCA 4.2.1 package [54]. All structures, monomer in the ground and excited states and dimers in the ground state, were optimized with the DFT method based on the PBE functional [55] and def2-SVP basis set [56] in the gas phase ($\varepsilon = 1$) with empirical Grimme correction D3BJ [57]. All the optimizations were confirmed to be stationary points by the analysis of the number of imaginary frequencies, found – not found for the minima. All spectrum calculations were performed in PBE0 functional [58] with def2-TZVP [56] basis set in DMF and DMF/water mixture solvents taken into account in the Polarizable Continuum Model (CPCM) [59]. The UV-Vis spectra based on the ground states geometry were calculated in time-dependent density-functional theory (TDDFT) [60] without the Tamm-Dancoff approximation. Additionally, absorption spectra based on the excited state dynamics were calculated in the adiabatic Hessian approximation, where both the ground state and the excited state geometries and Hessians are calculated in advance.

2.2 Sample Preparation

A metal complex AlClPc *stock solution* (Acros Organics, USA) with a concentration of 1.18×10^{-3} mol/l was prepared by dissolution of an AlClPc dry sample (weight of 0.0152 g) in 20 ml of DMF (Reakhim, Russia, double-distilled). The resulting concentration was determined from the electronic absorption spectra. The purity and individuality of crystalline AlClPc were confirmed using MALDI mass spectrometry on a Thermo DSQ II device (USA). The *stock solution* was stored in the dark at 4 °C and, if necessary, diluted before the experiment: 0.02 ml *stock solution* of metal complex AlClPc per 8 ml DMF, then *base solution*.

To study AlClPc aggregation behavior in DMF depending on different concentration of AlClPc we diluted 0.02 ml of *stock solution* in 1 ÷ 15 ml of DMF. Also, to study AlClPc aggregation behavior depending on different concentration of water in solution, we placed 2 ml of AlClPc *base solution* in a K10 standard quartz cuvette with a path length of 1 cm (to perform immediately spectrophotometric), and then 0.01 ÷ 1 ml of DMF-water solution (the DMF concentration was C_{DMF} = 4.7 vol.%) was sequentially added to the cuvette with an interval of 0.01 ml, by titration.

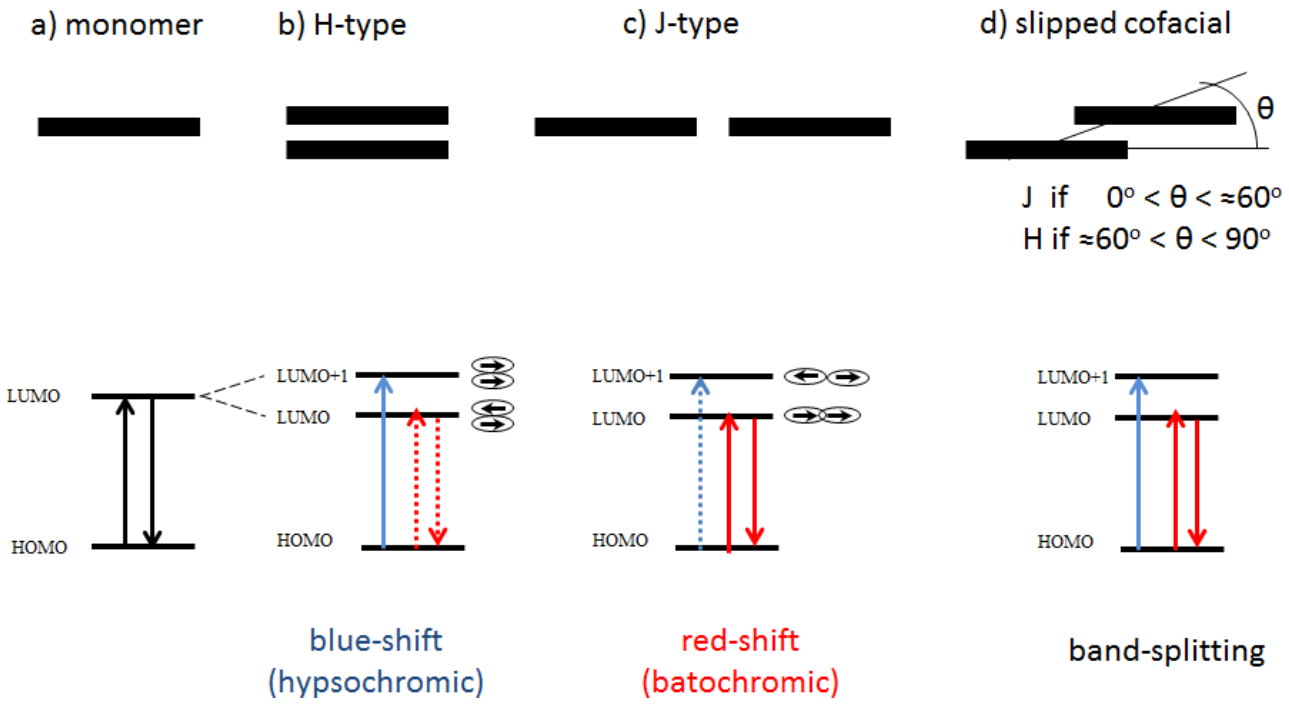

Fig. 1 Scheme of energy levels of MePc in monomer (a) and dimer (b–d) states with allowed (solid arrows) and prohibited (dotted arrows) transitions determined by parallel and antiparallel orientations of dipole transition moments.

2.3 Absorption and Fluorescence Spectroscopy

The UV-Vis absorption spectra were measured at room temperature in air using a TU-1901 UV-Vis spectrophotometer (Beijing Purkinje General Instrument Co. Ltd., China). The poorly resolved absorption spectra were analyzed by their decomposition into Gaussian components. Fluorescence measurements within 630−860 nm were performed with a Fluorat-02 Panorama spectrophotometer (Lumex, Russia). The excitation wavelength was 610 nm. All spectroscopy data were reduced to the initial value of the AlClPc-DMF solution volume.

3 Results and Discussion

3.1 The Classification of MePc Aggregates

According to the exciton coupling theory [61], MePc aggregates are classified as H-type, J-type and slipped cofacial structures depending on the mutual orientation of the molecules in MePc aggregates. The classification for dimers is illustrated in Fig. 1, where the molecules orientation and schematic energy levels are shown.

The long axis of an individual molecule in H-aggregates (Fig. 1(b)) is perpendicular to the axis of the aggregate ("face-to-face" stacked centrosymmetric structure). The transition between HOMO and LUMO levels is prohibited in H-type dimer due to the antiparallel orientations of dipole transition moments of individual molecules in dimer (see short arrows in ovals). That is why H-aggregate dimers show no detectable fluorescence. The lowest-energy allowed transition is between HOMO and LUMO + 1 levels. This band is blue-shifted and referred to as the H band ("H" for hypsochromic).

The long axis of an individual molecule in J-aggregates (Fig. 1(c)) is collinear to the axis of the aggregate ("head-to-tail" stacked). In contrast to H-aggregates, the transition between HOMO and LUMO levels is allowed. That is why J-aggregate dimers demonstrate fluorescence. This band is red-shifted and referred to as the J band ("J" is presumably for Jelley - one of the first researchers who investigate this red-shifted band).

Generally (Fig. 1(d)), the angle between the long axis of an individual molecule and the axis of the aggregate is between 0º and 90º (slipped cofacial structures). All transitions with different probabilities depending on the tilt angle θ are allowed in these dimers. There are both H- and J-bonds with different intensities in absorption spectra of slipped cofacial dimers. If θ is close to 90º, the H-band intensity is high and the J-bond intensity is low. If θ is close to 0º, the situation is vice versa. By convention, slipped cofacial structures refer to H-aggregates if θº≥ 60º, and slipped cofacial structures refer to J-aggregates if θ ≤ 60º.

Due to the structural features, H-aggregates of MePc are formed in many systems and they are not photoactive, while J-aggregates are formed much rarely and could be photoactive [62–65]. There are few works on red- and blue-shifted adsorption and red-shifted fluorescent spectra of Pc dimers [65–68].

3.2 Theoretical Calculations of AlClPc Monomer and Dimers Ground State

The ground state structures of possible types of dimers as well as those of monomer were calculated in gas-phase and DMF and DMF–water solution to elucidate the AlClPc aggregation in water and water-organic solutions.

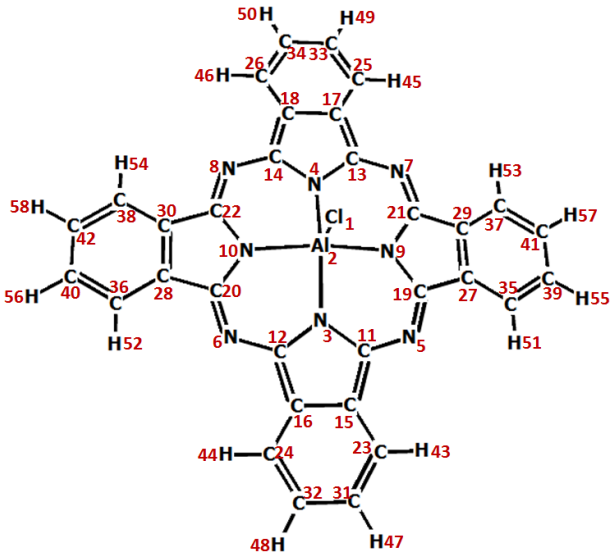

Fig. 2 Optimized structure of AlClPc monomer with atomic numbers.

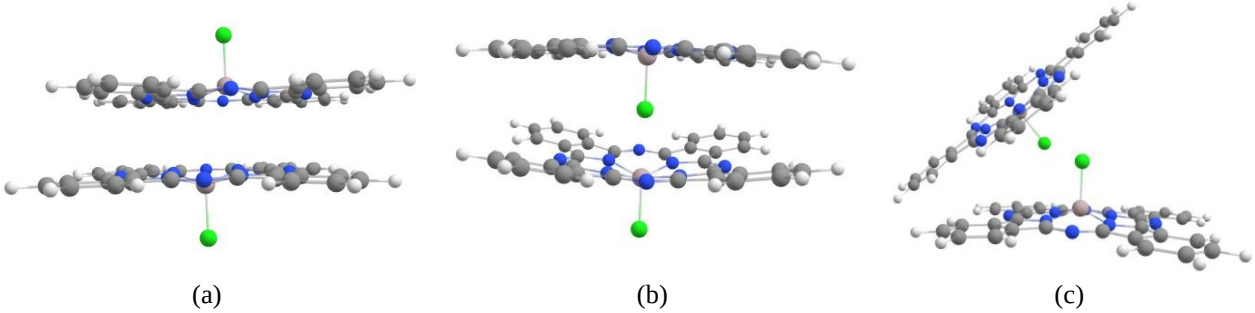

(a) (b) (c)

Fig. 3 Optimized geometries of AlClPc dimers with: (a) "back-to-back", (b) "back-to-face", and (c) "face-to-face" arrangements.

Table 1 AlClPc monomer structure parameters obtained by PBE/def2-SVP DFT calculations and X-ray diffraction data [69].

Parameter	DFT calculation	X-Ray	Parameter	DFT calculation	X-Ray
Bond lengths, Å					
Al_2–Cl_1	2.16	2.18	C_{15}–C_{16}	1.41	1.36
Al_2–N_3	2.00	1.98	C_{15}–C_{23}	1.40	1.46
N_3–C_{11}	1.39	1.44	C_{23}–C_{31}	1.40	1.41
C_{11}–C_{15}	1.46	1.37	C_{31}–C_{32}	1.41	1.41
N_5–C_{11}	1.33	1.36			
Bond angles, degree					
N_3–Al_2–Cl_1	103	103	C_{11}–C_{15}–C_{16}	106	109
C_{11}–N_3–Al_2	126	122	C_{16}–C_{15}–C_{23}	121	122
C_{11}–N_3–C_{12}	108	106	C_{15}–C_{23}–C_{31}	117	116
N_3–C_{11}–C_{15}	110	109	C_{23}–C_{31}–C_{32}	121	122
C_{11}–N_5–C_{19}	127	126			
Dihedral angles, degree					
Al_2–N_3–C_{11}–C_{15}	167	165	N_3–C_{11}–C_{12}–C_{16}	179	174
C_{11}–C_{15}–C_{16}–C_{24}	179	175	N_5–C_{11}–C_{19}–N_9	177	176

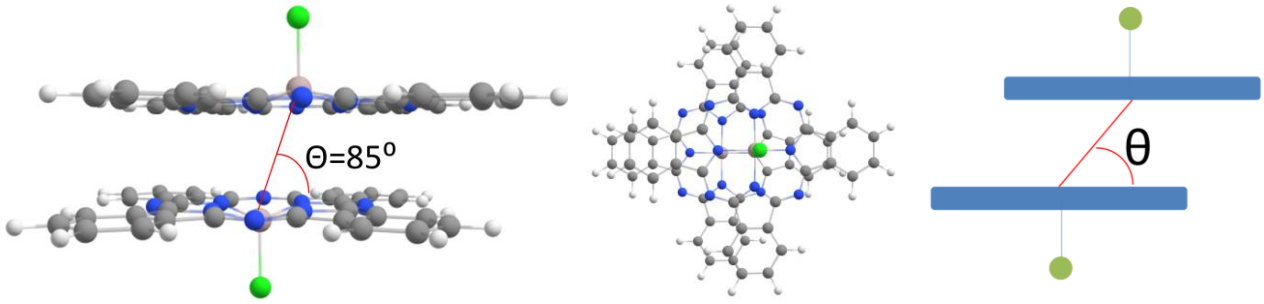

(a) (b) (c)

Fig. 4 Dimer of AlClPc with two molecules slightly dislocated: a) side view, b) top view, and c) scheme of slipped cofacial structures: $0 < \theta < 55°$ in J-aggregates and $55° < \theta < 90°$ in H-aggregates.

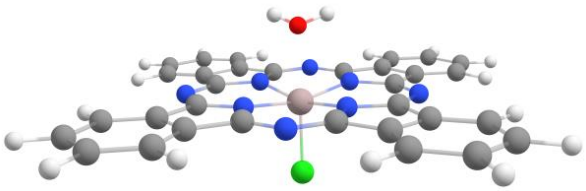

Fig. 5 Bounded AlClPc and H_2O molecules.

The AlClPc monomer with atomic numbering is shown in Fig. 2. The structure parameters of optimized monomer geometry are shown in Table 1, as well as X-ray diffraction literature data [69]. Table 1 demonstrates a good agreement between the calculated ground state AlClPc monomer geometry and the experimentally obtained [69] X-ray diffraction results. All geometries below are optimized in gas because of good reproduction of the experimental molecule parameters when calculating in the gas phase at an adequate cost of computer resources. It was shown that the spectra calculated on the geometry in DMF differ little from the spectra calculated on the gas-phase geometry.

Three different confirmations of dimer can be constructed for the AlClPc molecule, which have (a) “back-to-back”, (b) “back-to-face”, and (c) “face-to-face” arrangements, as illustrated in Fig. 3. Calculations show that “back-to-back” conformation is the most favorable. It is 19.7 and 20.6 kcal/mol lower than “back-to-face” and “face-to-face” conformations, respectively.

This AlClPc dimer is very similar to that of ZnPc [70]. The molecules in AlClPc dimer maintain the monomer geometry (Fig. 4), as in the ZnPc dimer. They are shifted relative to each other, and the aluminum is located above one of the nitrogens of the other molecule. As a result, a slipped cofacial aggregation is formed. The geometric parameters of each AlClPc in the dimer are similar to that in the monomer, and the intermolecular distance is *ca.* 3.7 Å. The energy of the dimer formation is *ca.* −40.7 kcal/mol, calculated as the difference between the dimer energy and twice energy of the monomer.

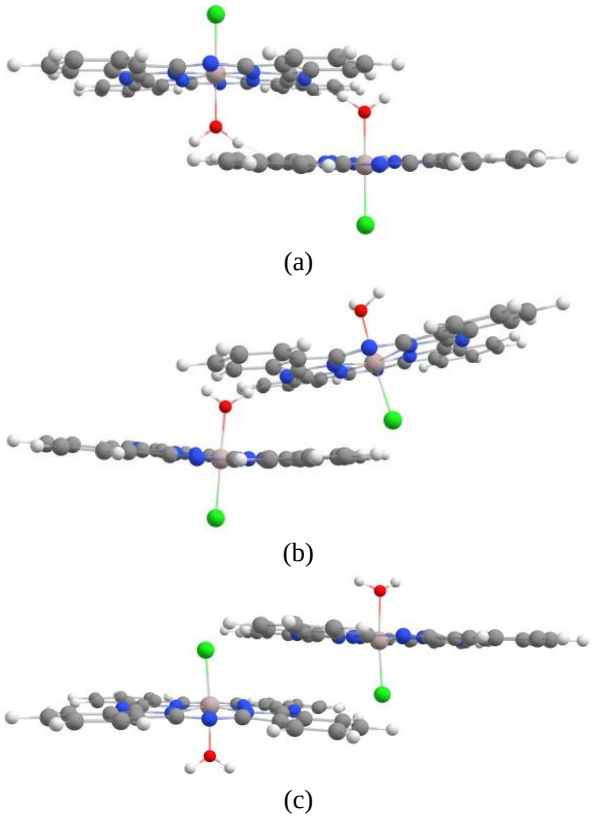

(a)

(b)

(c)

Fig. 6 Optimized geometries of bonded by two H_2O molecules AlClPc dimers with: (a) "back-to-back", (b) "back-to-face", and (c) "face-to-face" arrangements.

These results show that the lone nitrogen pair is involved in the formation of the AlClPc dimer, as in the case of the ZnPc dimer [70]. The stability of the dimer is due to the intermolecular coordination N → Al, since Al is partially positively charged in the AlClPc molecule. Thus, according to Kasha's exciton theory, the AlClPc dimer belongs to slipped coaficial structure with θ = 85º, i.e. AlClPc dimer can be referred to none-fluorescent H-aggregates [61]. Below, the AlClPc dimer is denoted by $[AlClPc]_2$.

In water-containing solvents, the AlClPc molecule easily binds to one H_2O molecule (Fig. 5) with the formation of a coordination bond between the Al atom of AlClPc and the O atom of the water molecule. The bond length is 2.23 Å and the hydration energy is −16.84 kcal/mol.

Hydrated AlClPc molecules can also form dimers with (a) "back-to-back", (b) "back-to-face", and (c) "face-to-face" arrangements, as illustrated in Fig. 6. Calculations show "back-to-back" arrangement in dimer with the lowest energy (Fig. 6(a)). It is stabilized by four bonds between two AlClPc molecules and two water molecules. Each water molecule has two bonds, one of them is a coordination bond between the O atom of the molecule and the Al atom of the AlClPc molecule, and one hydrogen bond is between the H atom of the molecule and the N atom of the other AlClPc molecule. Below, this AlClPc dimer is denoted by $[AlClPc\_H_2O]_2$. $[AlClPc\_H_2O]_2$ and belongs to slipped coaficial structure with θ = 28º, i.e. $[AlClPc\_H_2O]_2$ can be referred to short-fluorescent J-aggregates [61]. Side and top views of $[AlClPc\_H_2O]_2$ are shown in Fig. 7. The distance between AlClPc molecules in dimer is 3.15 Å.

3.3 Optical Absorption of AlClPc in DMF and DMF-Water Solution

The linear optical spectra of AlClPc in DMF and DMF-water solution in the excited state were analyzed to understand the types of interactions between AlClPc molecules in solutions. Generally, two strong optical absorption regions in the UV-Vis spectra of MePc are mainly caused by the π-electron transition on the conjugated system of Pc. The central metals have a significant effect on the position and intensity of the absorption maxima in the MePc UV-Vis spectra since the delocalization of the π-bond and d-orbitals of the metal in the MePc molecule is influenced by solvent molecules, which leads to a change in the shape and position of the B-band (or Soret band) and the Q-band [32]. According to Davydov's theory the Q-band splitting, the value is a characteristic of interaction energy between molecules with different site symmetries [71].

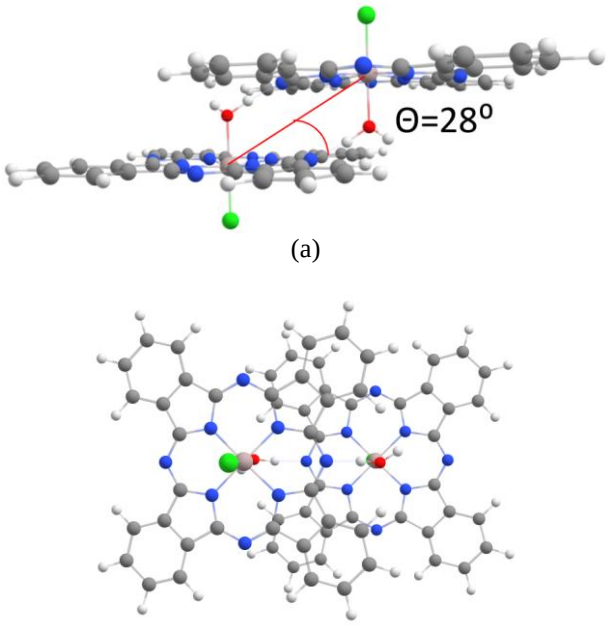

(a)

(b)

Fig. 7 Dimer of AlClPc, with the two molecules linked through two H_2O molecules: a) side view, b) top view.

The typical Q-band and B-band absorptions in the spectra for AlClPc in DMF and DMF-water solutions (Fig. 8) are in good agreement with those in Refs. [17, 32, 50, 62, 72]. In the absorption spectrum of AlClPc in DMF solution (Fig. 8, curve 1) there are two-principle π-π* transitions from the highest occupied molecular orbital (HOMO) to the lowest unoccupied molecular orbital (LUMO) of the metal complex: the B-band located at 300–450 nm with an absorption maximum at 349 nm, attributed to the a_{2u} (π) → e_g (π*)

transition, which is a characteristic of all MePc, and stronger Q-band located at 600–700 nm with an absorption maximum at λ_{QI} = 673 nm and a shoulder at λ_{QII} = 640 nm, which is a characteristic of all Pc and it is responsible for the colour of the compound. The latter absorption maximum at λ_{QI} = 673 nm is attributed to the $a_{1u}(\pi) \rightarrow e_g(\pi^*)$ transition, as well as its vibrational satellite of low intensity with an absorption maximum at λ_{QIII} = 607 nm, and it is a characteristic of the monomeric form of the AlClPc. At a high Pc concentration, the shoulder at ~ 640 nm transforms into a broader band, the intensity of which increases with the increase of the Pc concentration. The authors [73, 74] attribute this band to H-aggregates and explain a growth of the absorption at ~ 640 nm by dimerization / aggregation of the Pc at higher Pc concentrations. The absence of absorption in the long-wavelength region of the spectrum at λ = 710–850 nm (Fig 8, curve 1) indicates the absence of AlClPc J-aggregates in DMF.

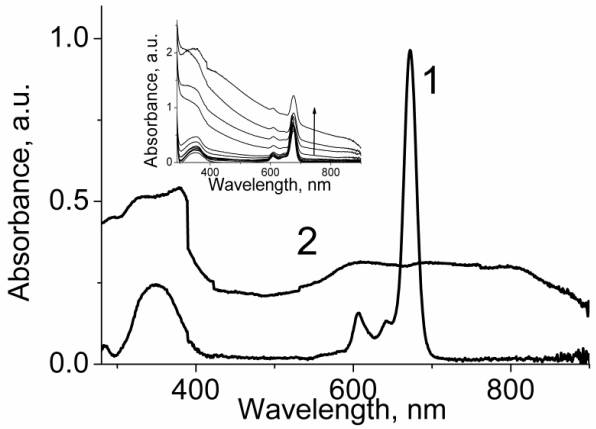

Fig. 8 UV-Vis spectra of AlClPc in DMF (1) and DMF-water mixture (C_{H2O} = 15 vol. %) (2). Inset: UV-Vis spectra of AlClPc in DMF-water solution with different concentration of water (C_{H2O} = 1.2 ÷ 11.1 vol. %); the arrow shows the increase in C_{H2O}.

As expected, the optical absorption of AlClPc in DMF-water solution (Fig. 8, curve 2) differs significantly from the same in DMF solution. There is a sharp decrease in the intensity of the Q-band, a significant broadening of the spectrum lines, and a shift of the absorption spectrum maximum to the short-wave length region. These changes in absorption spectra are related to aggregating behavior of AlClPc in the presence of water and a sharp decrease of AlClPc monomers, which leads to a reduce in quantum yield of singlet oxygen and a decrease in photodynamic activity of Pc [17, 33, 73]. Moreover, the formation of rather rare J-aggregates of AlClPc is observed, as evidenced by the presence of absorption in the optical region of λ = 700–850 nm and the appearance of small peaks in the region of λ = 705–780 nm (Fig. 8, curve 2). An insert describing the behavior of AlClPc in the presence of water indicates the aggregation capacity of AlClPc in binary DMF-water mixtures. With the increase of water concentration, the increase of scattering intensity is observed. At higher water amount in system (> 5 vol. %) the spectra show a complex multiple equilibrium between different types of AlClPc aggregates. The higher-order aggregates (J-type) are seen in a large number. It is known that scattering intensity is proportional to the size of aggregates [75]. So, we can state that aggregates increase in size with the increasing water concentration in system. Moreover, the presence of absorption at long wavelength region testifies a loss of symmetry in the AlClPc molecule due to the distortion of the MePc. This distortion of flat orientation is probably associated with the presence of oxygen in water and its interaction with Al.

3.4 Theoretical Calculations of AlClPc UV-Vis Absorption Spectra

The theoretical UV-Vis spectra were also calculated for monomer and both dimers in ground-state gas geometry for DMF and DMF-water in different proportions for better understanding of AlClPc aggregation and interpretation of the experimental spectra. It turned out that neither the positions of the peaks, nor the oscillator strengths are practically independent of the solvent. Moreover, the spectra are little sensitive to changes in the structural parameters. Also, the position of the peaks changes by no more than 0.5 nm at practically unchanged oscillator strengths when the optimized in DMF geometry is chosen instead of the optimized in gas.

Fig. 9 presents UV-Vis spectra of monomer and dimers in H-aggregate (see Fig. 4) and J-aggregate (see Fig. 7) forms normalized to the Q-band of monomer. Here, vertical lines present spectrum states and solid lines present the Gaussian broadening of the corresponding spectrum. The spectra were calculated in DMF for ground state geometries of corresponding structures, i.e. the spectra were calculated at T = 0 K without taking into account the electron-phonon interaction.

The peak at ~ 670 nm in the monomer spectrum corresponds to the Q-band related to the transition from the ground state to the first excited state. This is HOMO → LUMO transition (see orbitals in Fig. 10). The B-band (Soret) is presented by a series of peaks around ~ 330 nm.

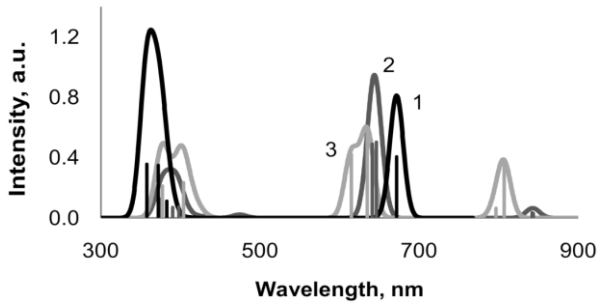

Fig. 9 Calculated absorption spectra of AlClPc monomer (1) and dimers in H-aggregate (2) and J-aggregate (3) forms in DMF.

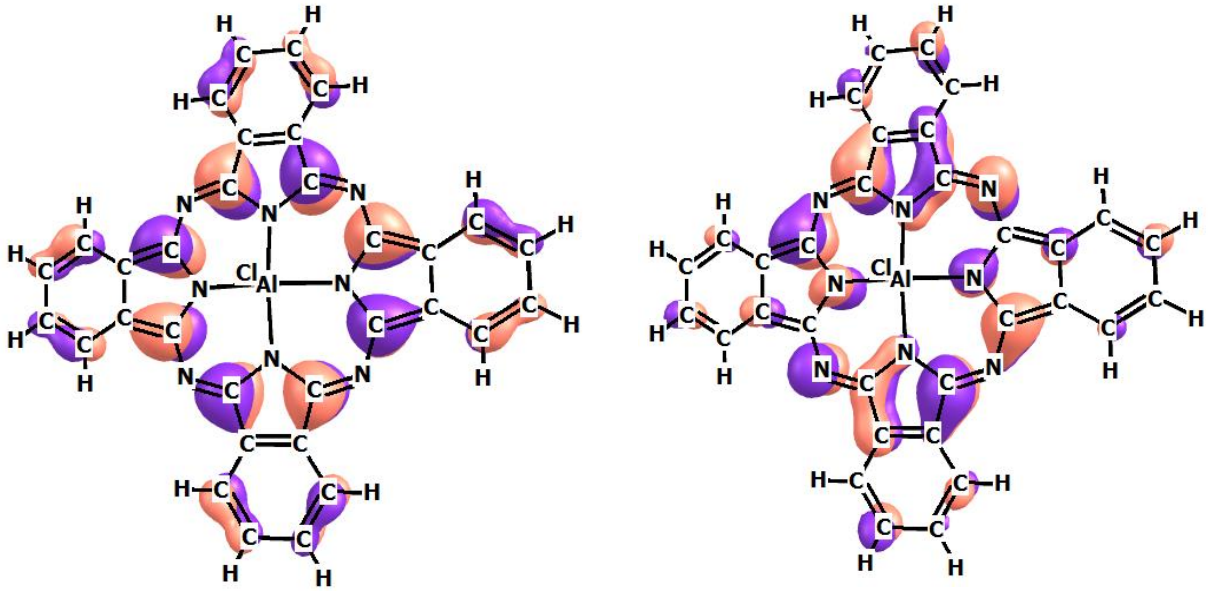

(a) (b)

Fig. 10 HOMO (a) and LUMO (b) orbitals of AlClPc.

The UV-Vis spectrum of H-aggregates is characterized by two high peaks in the spectrum region at ~ 640 nm and two low peaks in the spectrum region at ~ 840 nm. Since θ in H-aggregates is slightly less than 90 (θ = 85º, see Fig. 4), there is a low-intensity J-band (~ 840 nm), in addition to the high-intensity H-band (~ 640 nm), in the UV-Vis spectrum. The peaks at ~ 640 nm are the characteristics of the dimer; they are hypsochromically shifted with respect to the peak of the monomer. The peak at λ = 641 nm is presented by HOMO → LUMO + 3 transition with small contribution from HOMO − 1 → LUMO transition, and the peak at λ = 646 nm is presented by HOMO – 1 → LUMO + 2 transition with small contribution from HOMO → LUMO + 1 transition. The peaks at ~ 840 nm (λ = 841 and 842 nm) are the characteristics of the dimer; they are bathochromically shifted with respect to the peak of the monomer. They are symmetrical to the peaks at ~ 640 nm but with the inversion in contribution of transitions. The Soret band of the H-aggregate is located around 380 nm.

The calculated UV-Vis spectrum of J-aggregates differs from that of H-aggregates as the AlClPc molecules in J-aggregate are linked by two H_2O molecules. Since θ in J-aggregates is far from 0 (θ = 28º, see Fig. 7), both H-band and J-band in the spectra have high intensities. A hypsochromic shift of the absorption spectrum (H-band) with the formation of two well-separated peaks at 615 and 635 nm is observed, where the peak at 615 nm is presented by HOMO – 1 → LUMO + 3, and the peak at 635 nm is presented by HOMO – 1 → LUMO transition with small contribution from HOMO → LUMO + 2 transition. In the long wavelength spectrum region, the bathochromic shift (J-band) is detected with the formation of two peaks at ~ 797 and ~ 807 nm, while the peak at ~ 765 nm is low intensive. They are symmetrical to the peaks at ~ 615–635 nm but with the inversion in contribution of transitions. The Soret band of the J-aggregate is located around 390 nm as that of H-aggregates.

All calculated peaks in the Cope region are wide and overlap each other, so it is rather difficult to separate them in experimental spectra. Moreover, the peak at ~ 640 nm can indicate both H- and J-aggregates, since the latter have a strongly pronounced hypsochromic peak.

The spectra in Fig. 9 are superimposed on each other. However, in reality, the ratio of peak heights differs due to different concentrations of the components in the solution. Usually the concentration of J-aggregates is small, and concentration of H-aggregates depends on AlClPc concentration. Therefore, the intensities of J-aggregate peaks at ~ 800 nm are small, and their peaks at ~ 630 nm are not visible against the background of the peaks of the H-aggregate. Taking into account the different concentrations of monomers and H- and J-aggregates, Fig. 9 fairly well reflects the general picture of the adsorption spectrum in DMF, where the concentration of monomers is the largest, a small part of dimers is in the form of H-aggregates, and there are no J-aggregates.

According to Fig. 9 we can assume that both AlClPc H-aggregates and monomers influence the position of peaks and their intensity in the region of ~ 610–640 nm of the experimental spectrum (Fig. 8, curve 1). However, it is rather difficult to separate their contributions into the total absorption spectrum because of their overlap. Nevertheless, the presence of H-aggregates is highly improbable in the DMF-water system (Fig. 8, curve 2), since it is energetically favorable for AlClPc molecules to form J-aggregates with the help of two water molecules. In this case, the greater the amount of water is

in the system, the more AlClPc molecules are in the form of J-aggregates.

Electron-phonon interaction should be taken into account for better description of adsorption and emission spectra. In order to predict absorption or emission rates, including all vibronic transitions, ideally one needs both the ground state and excited state geometries and Hessians (matrix of the second-order partial derivatives of the molecule energy-function). Optimization of the excited state requires much more computer costs than optimization of the ground state. Therefore, we limited ourselves to calculating the most intensive Q-band in the monomer, which is of the most important interest from a practical point of view.

Fig. 11 presents monomer experimental and calculated absorption spectra in the region of Q-band. The theoretical spectrum was calculated in DFT/TDDFT without the Tamm-Dancoff approximation (TDA) for the first excited state at T = 298 K. The spectrum was calculated by the Adiabatic Hessian (AH) method, where the Hessians of both the ground and excited states are calculated in advance.

The Fig. 11 demonstrates excellent agreement between experiment and calculation. In the AlClPc spectrum, as well as in the ZnPc spectrum [65], there are two lower bands related to vibronic transitions at ~ 610 nm (Q_{III}) and ~ 640 nm (Q_{II}). The excellent agreement between the experimental adsorption spectrum in the range of 550–750 nm and the Q-band calculated in the adiabatic approximation indicates the presence of almost only monomers in DMF at experimental AlClPc concentrations of $C_{AlClPc} = 2.9 \times 10^{-6}$ mol/l (Fig. 8, curve 1). Thus, the calculated data (Fig. 11) fully confirm the conclusion on the absence of both H- and J- AlClPc aggregates in the DMF solution drawn from the experimental data (Fig. 8, curve 1).

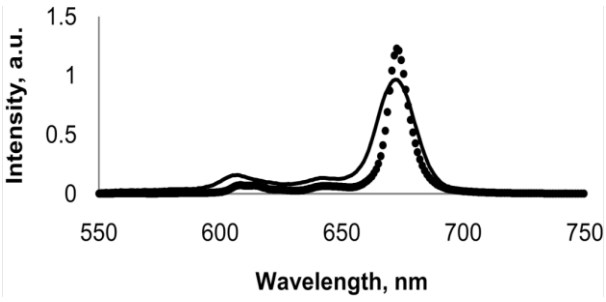

Fig. 11 Absorption spectrum of AlClPc monomer in the region of Q-band including the vibronic transitions: experiment (solid) and TD-DFT calculation (dots).

3.5 Fluorescence of AlClPc in DMF and DMF-Aqua Solution

Aggregation behavior of metal complex AlClPc in DMF was also studied by fluorescence spectroscopy. Fig. 12 shows the fluorescence spectra of AlClPc in DMF at different concentrations of the dye. As seen, AlClPc in DMF demonstrates high fluorescence intensity with excitation wavelength $\lambda_{ex} = 610$ nm. At high concentrations of AlClPc in DMF ($C_{AlClPc} = 2.3 \times 10^{-5}$ mol/l), the AlClPc fluorescence maximum is at ~ 687 nm. When the concentration of AlClPc in DMF decreases (from $C_{AlClPc} = 2.3 \times 10^{-5}$ mol/l to $C_{AlClPc} = 2.3 \times 10^{-6}$ mol/l), there is a blue shift in fluorescence maximums from 687 nm to 679 nm, which indicates that the concentration of Pc in DMF solution is an essential parameter.

Moreover, according to Ref. [65], it can be assumed that the change in the Pc concentration leads to an increase or suppression of fluorescence from different emission bands, and, possibly, the form of fluorescent curves detects various types of Pc aggregates in solution. For example, at higher concentrations of AlClPc in solution (~ 10^{-5} mol/l), pronounced shoulders around the main peak are the characteristics of aggregates, probably dimers, and at dye concentrations $C_{AlClPc} > 5 \times 10^{-6}$ mol/l dimers predominate. However, fluorescence dimers are very rare, and they are of J-type aggregate, so, it might be supposed that J-type dimers prevail in AlClPc-DMF solution with a $C_{AlClPc} > 5 \times 10^{-6}$ mol/l.

This conclusion is well consistent with the data obtained from the calculated optical absorption spectra (Fig. 9 and Fig. 11). Thus, this fact suggests that all experimentally obtained maxima on the absorption spectrum in the Q region can be safely attributed to bands characterizing the monomeric shape of the dye.

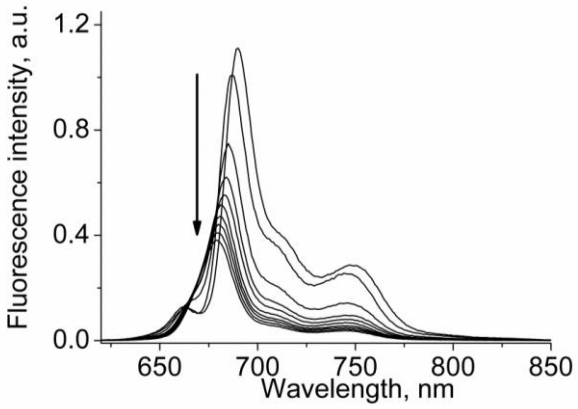

Fig. 12 The fluorescence spectra of AlClPc in DMF. $C_{AlClPc} = 2.3 \times 10^{-6}$ mol/l ÷ 2.3×10^{-5} mol/l. $\lambda_{ex} = 610$ nm. The arrow shows the decrease in AlClPc concentration.

At lower AlClPc concentrations in DMF solution ($< 5 \times 10^{-6}$ mol/l) a significant amount of the dye is in the monomeric form (Fig. 12). However, in our experiments, we did not reach the C_{AlClPc} at which the position of the fluorescence maximum remains unchanged, indicating that all AlClPc molecules are in monomeric form. Nevertheless, the position of the fluorescence maximum at $C_{AlClPc} < 3 \times 10^{-6}$ mol/l changes insignificantly, which indicates the predominance of the monomeric form of the dye in the DMF solution.

It is also known that the spectral position of all luminescence bands shifts to the short-wavelength region of the spectrum as the particle size decreases. A blue shift in fluorescence maximums with decreasing AlClPc

concentration also indicates the quantitative reduction of dimers and the predominance of monomers at low AlClPc concentrations in DMF solution.

The fluorescence spectra of AlClPc in DMF-water solution at different concentrations of aqua are shown in Fig. 13.

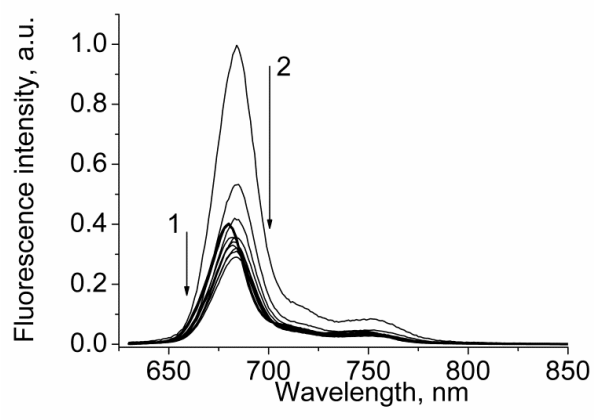

Fig. 13 The fluorescence spectra of AlClPc in DMF-water solution. C_{H20} = 0 ÷ 12.3 vol. %. λ_{ex} = 610 nm. The arrows show the increase in water concentration: (1) from 0 to 6.7 vol. %, (2) from 7.8 to 12.3 vol. %.

Unlike the data in Fig. 12, we observe a red shift of the fluorescence maximum AlClPc in DMF-water solution ($C_{AlClPc} = 2.9 \times 10^{-6}$ mol/l) with the increasing of water concentration in the system from 680 nm (C_{H2O} = 0 vol. %) to 684 nm (C_{H2O} = 5.6 vol. %) that indicates the aggregation process and the reduction of monomers in the system in this water concentration region (Fig. 13). Then, up to the water concentration in the system of C_{H2O} = 12.3 vol. %., the position of the fluorescent maximum does not change. Also, the shape of the fluorescence spectrum of AlClPc in a DMF-water solution differs from the shape of the dye spectrum in pure DMF.

We did not observe peak splitting at ~ 650–675 nm, as in Fig. 12, that indicates that the formation of dimers (aggregates) of the same nature occurs immediately, without the formation of intermediates. Also, we observed a drop in the luminescence intensity with an increase in the water concentration in the system from (C_{H2O} = 0 vol. %) to C_{H2O} = 7.8 vol. %. Then the intensity increases sharply, followed by a fall. Consequently, it might be supposed that there is a strong influence of the water concentration upon the aggregation state of the AlClPc, indicating, also, that there is a critical concentration of water when the ratio of monomers and dimers (J-aggregates) in the system changes dramatically.

When water is added to the system up to C_{H2O} = 6.7 vol. % the decrease in the fluorescence intensity and a shift in the fluorescence maximum towards long wavelengths testify to decreasing gradually the amount of AlClPc monomers and the simultaneous appearance of aggregates. It is hard to separate the input of monomers and aggregates to the general spectrum. However, since the fluorescence intensity sharply increases at C_{H2O} = 7.8 vol. %, it can be assumed that the amount of monomers in the system has sharply decreased due to AlClPc dimerization and formation of fluorescent J-aggregates.

The dependence of the monomeric AlClPc fraction on the water content was calculated by the method proposed in Refs. [73, 76, 77] based on the Gaussian decomposition of the data presented in Fig. 8 and taking into account the material balance equations $2C_m \leftrightarrow C_d$ and $C_0 = C_m + C_d$, where C_0, C_m and C_d are the total concentration of AlClPc and the concentration of monomers and dimers in the system, respectively. C_d and C_m in the mixed solution were determined from the equation for the total absorbance of the solution $D_0 = \varepsilon_0 \times C_0 = \varepsilon_m \times C_m + \varepsilon_d \times C_d$, where ε_0, ε_m, and ε_d are the observed molar extinction coefficient and molar extinction coefficients of monomers and dimers at a certain wavelength, respectively. The concentration of monomers C_m in the system with water was determined from the ratio $C_m = C_0 \times [(\varepsilon_0 - \varepsilon_d)/(\varepsilon_m - \varepsilon_d)]$. Thus, assuming that the proportion of monomers in the solution $f_m = C_m/C_o$, we obtained, that f_m decreases when water is added to the system and remains substantially unchanged up to C_{H2O} = 7.8 vol. %, with an average value of 90%. With a further increase in the water concentration there is a decrease in f_m (for example, at C_{H2O} = 11.2 vol. % the f_m = 0.7). The data obtained confirm the conclusion drawn from the fluorescence data analysis (Fig. 12, Fig. 13) and also indicate the presence of a critical water concentration in the system, at which the ratio of monomers and dimers changes dramatically.

3.6 Theoretical Calculations of AlClPc UV-Vis Fluorescence Spectrum

The calculated (T = 298 K) and experimental ($C_{AlClPc} = 2.9 \times 10^{-6}$ mol/l) fluorescence spectra are shown in Fig. 14. In contrast to the adsorption spectrum (Fig. 11), the calculated fluorescence spectrum does not show exact agreement with the experimental one. This is due to the features of the solvent continuum model, where the parameters are selected for better reproduction of the molecular ground state. Since the absorption spectrum is calculated as a vertical transition on the ground state geometry, it is quite well reproduced with an appropriate choice of functional and basis set.

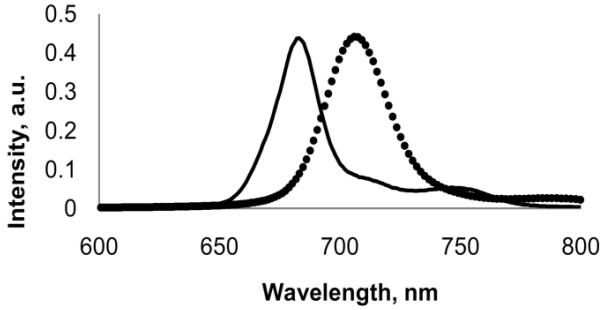

Fig. 14 Fluorescence spectrum of AlClPc monomer: experiment (solid) and TD-DFT calculation (dots).

The fluorescence spectrum is calculated on the geometry of the excited state. Since the continuum solvent model does not take into account the reorganization of the solvent under the transition from the ground state to the excited state. Moreover, the accuracy of the calculation of the fluorescence spectrum is worse than the accuracy of the calculation of the adsorption spectrum. Nevertheless, the calculated fluorescence spectrum reproduces the Stokes shift towards longer wavelengths. As the Stokes shift is primarily the result of vibrational relaxation and solvent reorganization, and the Pc molecule is a dipole surrounded by solvent molecules in a specific orientation, so the dipole moment of the molecule changes upon absorption of a photon and transition to an excited state. Part of the energy gained under the photon absorption is spent on rearranging the orientation of the solvent molecules. Therefore, the emitted photon has a lower energy than the absorbed one, and a shift towards longer wavelengths is observed in the fluorescence spectrum.

4 Conclusion

In this work, we studied the process of AlClPc aggregation in order to reveal differences in the behavior of the dye in organic and water-organic media.

Bearing in mind that AlClPc is being investigated as an effective Pc for PDT, the intensity of absorption in the infrared and visible regions and the ease of controlling the fluorescence maximum, achievable by changing the concentration of the dye in the solution are the important characteristics in the chemistry of Pc. All experimental and theoretical studies show the dependence the photophysical parameters of AlClPc on its aggregation properties and the monomer-dimer ratio in solutions, that are determined by the dye concentration in the medium.

It has been shown that in water-organic media the metal cation in the AlClPc molecule becomes six-coordinated, with two extraligands directed on opposite sides of the Pc macrocycle plane. Reduced solubilization capacity of the water-organic medium stimulates aggregation of MePc. Thus, along with the monomer, the spectra contain Pc dimers differing in structure. The higher the concentration of Pc in the solution and the greater the proportion of water in the water -DMF binary system, the higher the degree of Pc aggregation. Moreover, the simultaneous existence of AlClPc molecules in both forms (monomer/aggregates) is observed, as well as transitions between these states depending on the water and C_{AlClPc} concentrations in system. A critical concentration of water in system (~ 7.8 vol. %) when the ratio of monomers and dimers (J-aggregates) of AlClPc changes dramatically has been determined.

A different picture is observed when AlClPc is dissolved in pure DMF. In this case, Pc is completely in monomeric form. This solvatochromic effect also makes it possible to predict the aggregation behavior of AlClPc complexes in various media in hybrid materials, as well as to control and manage their aggregation behavior.

Acknowledgements

This research was supported by the IBCP RAS State Targets Project # 122041400110-4. We thank the Joint Supercomputer Center of the Russian Academy of Sciences (JSCC RAS) for providing computer resources for quantum calculations.

Disclosures

The authors declare no conflict of interest.

References

1. I. Rosenthal, “Phthalocyanines as photodynamic sensitizers,” Photochemistry and Photobiology 53, 859–870 (1991).
2. I. V. Klimenko, A. V. Lobanov, “Photosensitizing properties of supramolecular systems based on chlorin e6,” Journal of Biomedical Photonics & Engineering 2(4), 040310 (2016).
3. Z. Zhou, J. Song, L. Nie, and X. Chen, “Reactive oxygen species generating systems meeting challenges of photodynamic cancer therapy,” Chemical Society Reviews 45, 6597–6626 (2016).
4. L. Lin X. Song, X. Dong, and B. Li, “Nano-photosensitizers for enhanced photodynamic therapy,” Photodiagnosis and Photodynamic Therapy 36, 102597 (2021).
5. S. B. Brown, T. G. Truscott, “New light on cancer therapy,” Chemistry in Britain 29(11), 955–958 (1993).
6. R. Bonnett (Ed.), Chemical Aspects of Photodynamic Therapy, Gordon and Breach Science Publishers, Amsterdam (2000). ISBN 90-5699-248-1.
7. A. Ogunsipe, T. Nyokong, “Effects of central metal on the photophysical and photochemical properties of non-transition metal sulfophthalocyanine,” Journal of Porphyrins and Phthalocyanines 9(2), 121–129 (2005).
8. Z. A. Carneir, J. C. de Moraes, F. P. Rodrigues, R. G. de Lima, C. Curti, Z. N. da Rocha, M. Paulo, L. M. Bendhack, A. C. Tedesco, A. L. B. Formiga, and R. S. da Silva, “Photocytotoxic activity of a nitrosyl phthalocyanine ruthenium complex – A system capable of producing nitric oxide and singlet oxygen,” Journal of Inorganic Biochemistry 105(8), 1035–1043 (2011).
9. C. Jing, R. Wang, H. Ou, A. Li, Y. An, S. Guo, and L. Shi, “Axial modification inhibited H-aggregation of phthalocyanine in polymeric micelles for enhanced PDT efficacy,” Chemical Communications 54(32), 3985–3988 (2018).

10. A. Braun, J. Tcherniac, "Uber die Produckte der Einwirkung von Acetanhydrid auf Phthalamid," Berichte der deutschen chemischen Gesellschaft 40(2), 2709–2714 (1907).
11. H. S. Nalwa (Ed.), Supramolecular Photosensitive and Electroactive Materials, 1st ed., San Diego, USA (2001). ISBN: 9780080542119.
12. M. van Leeuwen, A. Beeby, I. Fernandes, and S. H. Ashworth, "The photochemistry and photophysics of a series of alpha octa(alkyl-substituted) silicon, zinc and palladium phthalocyanines," Photochemical & Photobiological Sciences 13, 62–69 (2014).
13. C. G. Claessens, U. Hahn, and T. Torres, "Phthalocyanines: From Outstanding Electronic Properties to Emerging Applications," The Chemical Record 8(2), 75–97(2008).
14. F. Cong, B. Ning, Y. Ji, X. Wang, F. Ke, Y. Liu, X. Cui, and B. Chen, "The facile synthesis and characterization of tetraimido-substituted zinc phthalocyanines," Dyes and Pigments 77(3), 686–690 (2008).
15. R. Medyouni, B. Hallouma, L. Mansour, S. Al-Quraishy, and N. Hamdi, "DBU-catalysed synthesis of metal-free phthalocyanines and metallophthalocyanines containing 2(3,4-dimethoxyphenyl)ethanol and 4-hydroxybenzaldehyde groups: characterisation, antimicrobial properties and aggregation behaviour," Journal of Chemical Research 41(5), 291–295 (2017).
16. T. M. Tsubone, G. Braga, B. H. Vilsinski, A. P. Gerola, N. Hioka, A. L. Tessaro, and W. Caetano, "Aggregation of Aluminum Phthalocyanine Hydroxide in Water/Ethanol Mixtures," Journal of the Brazilian Chemical Society 25(5), 890–897 (2014).
17. I. V. Klimenko, E. A. Trusova, A. N. Shchegolikhin, A. V. Lobanov, and L. V. Jurina, "Surface modification of graphene sheets with aluminum phthalocyanine complex," Fullerenes, Nanotubes and Carbon Nanostructures 30(1), 133–139 (2022).
18. J. M. Dąbrowski, L. G. Arnaut, "Photodynamic therapy (PDT) of cancer: from a local to a systemic treatment," Photochemical & Photobiological Sciences 14(10), 1765–1780 (2015).
19. K. Palewska, J. Sworakowski, and J. Lipiński, "Molecular aggregation in soluble phthalocyanines – chemical interactions vs. π-stacking," Optical Materials 34(10), 1717–1724 (2012).
20. I. R. Calori, A. C. Tedesco, "Lipid vesicles loading aluminum phthalocyanine chloride: Formulation properties and disaggregation upon intracellular delivery," Journal of Photochemistry and Photobiology B: Biology 160, 240–247 (2016).
21. M.-S. Liao, S. Scheiner, "Electronic Structure and Bonding in Metal Phthalocyanines, Metal = Fe, Co, Ni, Cu, Zn, Mg," The Journal of Chemical Physics 114(2), 9780−9791 (2001).
22. X. Lu, K. W. Hipps, X. D. Wang, and U. Mazur, "Scanning tunneling microscopy of metal phthalocyanines: d7 and d9 cases," Journal of the American Chemical Society 118(30), 7197−7202 (1996).
23. S. Feng, N. Luo, A. Tang, W. Chen, Y. Zhang, S. Huang, and W. Dou, "Phthalocyanine and metal phthalocyanines adsorbed on graphene: a density functional study," The Journal of Physical Chemistry C 123(27), 16614−16620 (2019).
24. J. Rak, P. Pouckova, J. Benes, and D. Vetvicka, "Drug delivery systems for phthalocyanines for photodynamic therapy," Anticancer Research 39(7), 3323–3339 (2019).
25. G. Swart, E. Fourie, and J. Swarts, "Octakis(dodecyl)phthalocyanines: Influence of Peripheral versus Non-Peripheral Substitution on Synthetic Routes, Spectroscopy and Electrochemical Behaviour," Molecules 27(5), 1529 (2022).
26. G. Gümrükçü, G. K. Karaoğlan, A. Erdoğmuş, A. Gül, and U. Avcıata, "Photophysical, Photochemical, and BQ Quenching Properties of Zinc Phthalocyanines with Fused or Interrupted Extended Conjugation," Journal of Chemistry 2014, 435834 (2014).
27. I. J. MacDonald, T. J. Dougherty, "Basic principles of photodynamic therapy," Journal of Porphyrins and Phthalocyanines 5(2), 105–129 (2001).
28. J. P. Mensing, C. Sriprachuabwong, A. Wisitsoraat, T. Kerdcharoen, and A. Tuantranont, "Phthalocyanine/graphene hybrid-materials for gas sensing in bio-medical applications," in the 4th 2011 Biomedical Engineering International Conference, 29–31 January 2012, Chiang Mai, Thailand, 190–193 (2012).
29. G. Zhang, Y. Zhang, A. Tan, Y. Yang, and M. Tian, "Effects of MN4- type coordination structure in metallophthalocyanine for bioInspired oxidative desulfurization performance," Molecules 27(3), 904 (2022).
30. M. Cavazzini, G. Pozzi, S. Quici, and I. Shepperson, "Fluorous biphasic oxidation of sulfides catalysed by (salen)manganese(III) complexes," Journal of Molecular Catalysis A: Chemical 204–205, 433–441 (2003).
31. M. J. Schultz, M. S. Sigman, "Recent advances in homogeneous transition metal-catalyzed aerobic alcohol oxidations," Tetrahedron 62(35), 8227–8241 (2006).
32. H. Cao, M. Gong, M. Wang, Q. Tang, L. Wang, and X. Zheng, "Steady/transient state spectral researches on the solvent-triggered and photo-induced novel properties of metal-coordinated phthalocyanines," RSC Advances 12(10), 5964–5970 (2022).
33. A. Jlali, C. Jablaoui, M. Lahouel, and B. Jamoussi, "New Zinc (II) Phthalocyanines Substituents: Synthesis, Characterization, Aggregation Behavior, Electronic and Antibacterial Properties," International Journal of Science and Research 5, 1750–1756 (2016).

34. N. B. Sul'timova, P. P. Levin, A. V. Lobanov, and A. M. Muzafarov, "Laser photolysis study of the triplet states of phthalocyanines on the surface of silica nanoparticles in aqueous solutions," High Energy Chemistry 47(3), 98–102 (2013).
35. K. Grodowska, A. Parczewski, "Organic solvents in the pharmaceutical industry," Acta Poloniae Pharmaceutica. Drug Research 67(1), 3–12 (2010).
36. E. I. Olivier, D. du Toit, and J. H. Hamman, "Development of an analytical method for the evaluation of N,N-dimethylformamide in dosage form design," Die Pharmazie-An International Journal of Pharmaceutical Sciences 62(10), 735–738 (2007).
37. E. A. Trusova, I. V. Klimenko, A. M. Afzal, A. N. Shchegolikhin, and L. V. Jurina, "Comparison of oxygen-free graphene sheets obtained in DMF and DMF-aqua media," New Journal of Chemistry 45(23), 10448–10458 (2021).
38. M. E. Alea-Reyes, M. Rodrigues, A. Serra, M. Mora, M. L. Sagrista, A. Gonzalez, S. Duran, M. Duch, J. A. Plaza, E. Valles, D. A. Russell, and L. Perez-Garcia, "Nanostructured materials for photodynamic therapy: synthesis, characterization and in vitro activity," RSC Advances 7(28), 16963–16976 (2017).
39. P. Vallecorsa, G. D. Venosa, M. B. Ballatore, D. Ferreyra, L. Mamone, D. Sáenz, G. Calvo, E. Durantini, and A. Casas, "Novel meso-substituted porphyrin derivatives and its potential use in photodynamic therapy of cancer," BMC Cancer 21, 547 (2021).
40. A. V. Lobanov, G. S. Dmitrieva, N. B. Sul'timova, and P. P. Levin, "Aggregation and Photophysical Properties of Phthalocyanines in Supramolecular Complexes," Russian Journal of Physical Chemistry B 8, 272–276 (2014).
41. N. A. Kuznetsova, N. S. Gretsova, V. M. Derkacheva, O. L. Kaliya, and E. A. Lukyanets, "Sulfonated phthalocyanines: aggregation and singlet oxygen quantum yield in aqueous solutions," Journal of Porphyrins and Phthalocyanines 7(03), 147–154 (2003).
42. C. C. Jayme, I. R. Calori, E. M. F. Cunha, and A. C. Tedesco, "Evaluation of aluminum phthalocyanine chloride and DNA interactions for the design of an advanced drug delivery system in photodynamic therapy," Spectrochimica Acta Part A: Molecular and Biomolecular Spectroscopy 201, 242–248 (2018).
43. N. S. Lebedeva, O. V. Petrova, A. I. Vyugin, V. E. Maizlish, and G. P. Shaposhnikov, "Peculiarities of solvation interaction of water-soluble metallophthalocyanines with ethanol," Thermochimica Acta 417(1), 127–132 (2004).
44. Q. Li, Z. Wang, Q. Liang, M. Zhou, S. Xu, Z. Li, and D. Sun, "Tetra-substituted cobalt (II) phthalocyanine/multi-walled carbon nanotubes as new efficient catalyst for the selective oxidation of styrene using tert-butyl hydroperoxide," Fullerenes, Nanotubes and Carbon Nanostructures 28(10), 799–807 (2020).
45. T. Nyokong, "Effects of substituents on the photochemical and photophysical properties of main group metal phthalocyanines," Coordination Chemistry Reviews 251(13-14), 1707−1722 (2007).
46. J. Janczak, "Water-involved hydrogen bonds in dimeric supramolecular structures of magnesium and zinc phthalocyaninato complexes," ACS Omega 4(2), 3673−3683 (2019).
47. H. K. Moon, M. Son, J. E. Park, S. M. Yoon, S. H. Lee, and H. C. Choi, "Significant increase in the water dispersibility of zinc phthalocyanine nanowires and applications in cancer phototherapy," NPG Asia Materials 4(4), e12 (2012).
48. F. L. Primo, M. M. A. Rodrigues, A. R. Simioni, M. V. L. B. Bentley, P. C. Morais, and A. C. Tedesco, "In vitro studies of cutaneous retention of magnetic nanoemulsion loaded with zinc phthalocyanine for synergic use in skin cancer treatment," Journal of Magnetism and Magnetic Materials 320(14), e211–e214 (2008).
49. O. I. Koifman, M. Hanack, S. A. Syrbu, and A. V. Lyubimtsev, "Phthalocyanine conjugates with carbohydrates: synthesis and aggregation in aqueous solutions," Russian Chemical Bulletin 62(4), 896–917 (2013).
50. M. A. Gradova, I. I. Ostashevskaya, O. V. Gradov, A. V. Lobanov, and V. B. Ivanov, "Photophysical properties and photochemical activity of metal phthalocyanines adsorbed on modified montmorillonite macroheterocycles," Macroheterocycles 11(4), 404–411 (2018).
51. E. P. O. Silva, E. D. Santos, C. S. Gonçalves, M. A. G. Cardoso, C. P. Soares, and M. Beltrame, "Zinc phthalocyanineconjugated with bovine serum albumin mediated photodynamic therapy of human larynx carcinoma," Laser Physics 26, 105601 (2016).
52. E. Güzel, A. Atsay, S. Nalbantoglu, N. Şaki, A. L. Dogan, A. Gül, and M. B. Koçak, "Synthesis, characterization and photodynamic activity of a new amphiphilic zinc phthalocyanine," Dyes and Pigments 97(1), 238–243 (2013).
53. I. V. Klimenko, A. V. Lobanov, E. A. Trusova, and A. N. Schegolikhin, "New hybrid oxygen-free graphene and phthalocyanine aluiminum structures: preparation and physicochemical properties," Russian Journal of Physical Chemistry B 13, 964–968 (2019).
54. F. Nees, F. Wennmohs, U. Becker, and C. Riplinger, "The ORCA quantum chemistry program package," The Journal of Chemical Physics 152(22), 224108 (2020).
55. J. P. Perde, K. Burke, and M. Ernzerhof, "Generalized gradient approximation made simple," Physical Review Letters 77(18), 3865–3868 (1996).
56. F. Weigend, R. Ahlrichs, "Balanced basis sets of split valence, triple zeta valence and quadruple zeta valence quality for H to Rn: Design and assessment of accuracy," Physical Chemistry Chemical Physics 7(18), 3297–3305 (2005).

57. S. Grimme, J. Antony, S. Ehrlich, and H. Krieg, "A consistent and accurate ab initio parametrization of density functional dispersion correction (DFT-D) for the 94 elements H-Pu," The Journal of Chemical Physics 132(15), 154104 (2010).
58. M. Ernzerhof, G. E. Scuseria, "Assessment of the Perdew-Burke-Ernzerhof exchange-correlation functional," The Journal of Chemical Physics 110(11), 5029–5036 (1999).
59. V. Barone, M. Cossi, "Quantum Calculation of Molecular Energies and Energy Gradients in Solution by a Conductor Solvent Model," The Journal of Physical Chemistry A 102(11), 1995–2001 (1998).
60. C. Adamo, D. Jacquemin, "The calculations of excited-state properties with time-dependent density functional theory," Chemical Society Reviews 42(3), 845–856 (2013).
61. M. Kasha, "Energy transfer mechanisms and the molecular exciton model for molecular aggregates," Radiation Research 20(1), 55–71 (1963).
62. A. V. Lobanov, N. B. Sul'timova, P. P. Levin, I. B. Meshkov, and M. Y. Melnikov, "Aluminum phthalocyanine on silica nanoparticles: aggregation and excited states," Macroheterocycles 8(3), 279–283 (2015).
63. K. Kameyama, M. Morisue, A. Satake, and Y. Kobuke, "Highly fluorescent self-coordinated phthalocyanine dimers," Angewandte Chemie International Edition 44(30), 4763–4766 (2005).
64. F. Würthner, T. E. Kaiser, and C. R. Saha-Möller, "J-Aggregates: From Serendipitous Discovery to Supramolecular Engineering of Functional Dye Materials," Angewandte Chemie International Edition 50(15), 3376–3410 (2011).
65. P. P. Pompa, G. Ciccarella, J. Spadavecchia, R. Cingolani, G. Vasapollo, and R. Rinaldi, "Spectroscopic investigation of inner filter effects by phthalocyanine solutions," Journal of Photochemistry and Photobiology A: Chemistry 163(1-2), 113–120 (2004).
66. S. FitzGerald, C. Farren, C. F. Stanley, A. Beeby, and M. R. Bryce, "Fluorescent phthalocyanine dimers—a steady state and flash photolysis study," Photochemical & Photobiological Sciences 1(8), 580–587 (2002).
67. A. Y. Tolbin, V. B. Sheinin, O. I. Koifman, and L. G. Tomilova, "Synthesis of stable dimeric phthalocyanine J-type complexes and investigation of their nucleophilic properties," Macroheterocycles 8(2), 150–155 (2015).
68. P. N. Vasilevsky, E. S. Davydova, D. I. Podshivalova, and M. S. Saveliev, "Nonlinear optical response of Phthalocyanine J-type dimeric complexes of Mg in DMF using pulsed femtosecond radiation," in 2021 IEEE Conference of Russian Young Researchers in Electrical and Electronic Engineering (ElConRus), 26–29 January 2021, Saint Petersburg, Moscow, Russia, 2902–2905 (2021).
69. T. Strenalyuk, S. Samdal, and H. V. Volden, "Molecular Structures of Chloro(phthalocyaninato)-aluminum(III) and -gallium(III) as determined by gas electron diffraction and quantum chemical calculations: quantum chemical calculations on fluoro(phthalocyaninato)-aluminum(III) and -gallium(III), chloro(tetrakis(1,2,5-thiadiazole)porphyrazinato)-aluminum(III) and -gallium(III) and comparison with their X-ray structures," The Journal of Physical Chemistry A 112(38), 9075–9082 (2008).
70. I. R. Calori, C. C. Jayme, L. T. Ueno, F. B. C. Machado, and A. C. Tedesco, "Theoretical and experimental studies concerning monomer/aggregates equilibrium of zinc phthalocyanine for future photodynamic action," Spectrochimica Acta Part A: Molecular and Biomolecular Spectroscopy 214, 513–521 (2019).
71. G. A. Kumar, J. Thomas, N. V. Unnikrishnan, V. P. N. Nampoori, and C. P. G. Vallabhan, "Optical properties of phthalocyanine molecules in cyano acrylate polymer matrix," Materials Research Bulletin 36(1–2), 1–8 (2001).
72. Z. Ou, J. Shen, and K. M. Kadish, "Electrochemistry of Aluminum Phthalocyanine: Solvent and Anion Effects on UV−Visible Spectra and Reduction Mechanisms," Inorganic Chemistry 45(23), 9569–9579 (2006).
73. A. W. Snow, "Phthalocyanine aggregation," in The Porphyrin Handbook: Phthalocyanines: Properties and Materials, K. M. Kadish, K. M. Smith, and R. Guilard (Eds.), Academic Press, San Diego, 129–176 (2003).
74. S. Dhami, D. Phillips, "Comparison of the photophysics of an aggregating and non-aggregating aluminium phthalocyanine system incorporated into unilamellar vesicles," Journal of Photochemistry and Photobiology A: Chemistry 100(1–3), 77–84 (1996).
75. J. Parkash, J. H. Robblee, J. Agnew, E. Gibbs, P. Collings, R. F. Pasternack, and J. C. de Paula, "Depolarized Resonance Light Scattering by Porphyrin and Chlorophyll a Aggregates," Biophysical Journal 74(4), 2089–2099 (1998).
76. D. A. Makarov, N. A. Kuznetsova, O. A. Yuzhakova, L. P. Savvina, O. L. Kaliya, E. A. Lukyanets, V. M. Negrimovskii, and M. G. Strakhovskaya, "Effects of the degree of substitution on the physicochemical properties and photodynamic activity of zinc and aluminum phthalocyanine polycations," Russian Journal of Physical Chemistry A 83, 1044–1050 (2009).
77. A. V Ziminov, V. K. Mal'tsev, A. A. Sherstyuk, Y. A. Vikent'eva, N. S. Seravin, and S. M. Ramsh, "Synthesis and aggregation of cationic zink and magnesium phthalocyanines containing 4-(3,5-dimethyl-1h-pyrazol-1-yl)phenoxy groups," Russian Journal of General Chemistry 88(8), 1648–1656 (2018).